The Astrophysical Journal, 668:594–602, 2007 October 10

ON THE CHARACTERISTICS OF THE SOLAR GRAVITY MODE FREQUENCIES

S. Mathur,[1,2] S. Turck-Chièze,[1,2] S. Couvidat,[3] and R. A. García[1,2]
Received 2007 April 17; accepted 2007 June 15

ABSTRACT

Gravity modes are the best probes for studying the dynamics of the solar radiative zone, and especially the nuclear core. This paper shows how specific physical processes influence the theoretical g-mode frequencies for the $\ell = 1$ and $\ell = 2$ modes over a large range of radial orders n from -46 to -1, corresponding to potential *SOHO* observations. To this end, we compute different solar models, and we calculate the corresponding theoretical g-mode frequencies. These frequencies are sensitive to the physical inputs of our solar models in the high-frequency range of the oscillation power spectrum. At low frequency, we demonstrate that the periodic spacing (ΔP_ℓ) between two g-modes with consecutive orders n and with the same angular degree ℓ does not vary significantly from one model to the other. For all the models considered, including models based on recent solar chemical abundances, the value of the characteristic quantity P_0, the fundamental period of the g-modes, is constant within a 1 minute range (between 34 and 35 minutes). This result is in sharp contrast to the situation before the launch of the *SOHO* spacecraft, when the dispersion for P_0 was large (with values ranging from 29 to 60 minutes). Then, we estimate the sensitivity of the oscillation frequency splittings to the solar core rotation. Finally, we review some features of the g-mode observations obtained with the GOLF instrument and based on an almost complete solar cycle. Some of these help us constrain the excitation mechanisms of g-modes.

Subject headings: Sun: helioseismology — Sun: interior — Sun: oscillations

Online material: color figures

1. INTRODUCTION

Gravity modes are a unique tool to constrain the rotation and density profiles of the solar core. In this paper, we attempt to develop theoretical bases to determine their intrinsic properties. These modes have been researched for more than 20 years (Hill et al. 1991; Turck-Chièze 2006, and references therein) and are still actively looked for in the data produced by the instruments located on board the *SOHO* spacecraft (Appourchaux et al. 2000; Gabriel et al. 2002). Recent analyses of these data unraveled g-mode candidates with a confidence level greater than 98% (Turck-Chièze et al. 2004a, 2004c), and detected a signature associated with their dipolar asymptotic properties with an even higher confidence level (García et al. 2007). These works stimulated the present paper, a dedicated theoretical study of g-mode properties.

In parallel with observational efforts, the quality of solar models has been improved during the last two decades thanks to tighter helioseismic constraints derived from p-mode detection. Major progress has been achieved in the description of the microscopic physics such as the opacities, the equation of state, and the nuclear reaction rates (Rogers & Iglesias 1994; Iglesias & Rogers 1996; Adelberger et al. 1998). The introduction of microscopic diffusion and of turbulence in the tachocline has significantly reduced the discrepancy between solar models and the observed solar sound-speed and density profiles (Christensen-Dalsgaard et al. 1993; Thoul & Bahcall 1994; Brun et al. 1998, 1999). Several works have been dedicated to modeling the radiative zone through combined seismic measurements (Turck-Chièze et al. 2001; Couvidat et al. 2003a), resulting in a solar model in good agreement with the helioseismic observations, commonly referred to as the seismic model. It was specifically constructed so that its sound-speed profile would match the observed solar profile in the radiative interior (i.e., the radiative zone including the nuclear core). This seismic model must be considered an intermediate step between a standard model (SSM), which neglects the dynamics of the solar interior, and a dynamic model (SDM), which is not yet complete. The dynamic model is expected to include both the effects of gravity waves and magnetic field, and to take into account the evolution of the internal radial rotation and its impact on the transport of angular momentum (Mathis & Zahn 2004, 2005; Charbonnel & Talon 2005; Brun & Zahn 2006; Palacios et al. 2006).

The seismic model slightly improves the prediction of the values of the neutrino fluxes (Turck-Chièze 2005a, 2005b) and of the g-mode frequencies, which are both sensitive to the structure of the radiative interior. Advantageously, this model produces theoretical g-mode frequencies that do not vary significantly with reasonable changes in the model inputs (Turck-Chièze et al. 2004b; Turck-Chièze 2005a, 2005b; Turck-Chièze & Talon 2007). The seismic model was based on the solar chemical abundances of Grevesse et al. (1993). In principle, it is possible to include more recent solar abundances for the CNO elements, as prescribed by Asplund et al. (2005). However, the resulting sound-speed profile is significantly altered by this change in abundances, and we need to decrease the opacities of the CNO elements to reduce the discrepancy between the model and the observed sound-speed profiles. When these two procedures (the new abundances and the reduced opacities) are combined, the neutrino fluxes remain unchanged. The seismic model was developed by the CEA/Saclay team and is an evolutionary model. It takes into account the impact of each chemical element on the opacity coefficients. Therefore, it differs from the seismic model of Shibahashi & Tamura (2006), which was directly derived from the observational constraints (solar radius, luminosity, and the seismic sound-speed profile) and from the basic stellar structure equations, without

[1] DAPNIA/CEA CE Saclay, FR-91191 Gif-sur-Yvette Cedex, France.
[2] AIM-Unité Mixte de Recherche CEA-CNRS-Université Paris VII-UMR 7158, FR-91191 Gif-sur-Yvette, France.
[3] HEPL, 455 via Palou, Stanford University, CA 94305-4085.

taking into account the dependence of the opacity coefficients on the proton number of each chemical species across the radiative interior (Turck-Chièze et al. 2005a).

Here we study the impact of the microscopic diffusion, the turbulence in the tachocline, and the chemical composition on the prediction of g-mode frequencies. This study helps to interpret the different observations of *SOHO*. We compute the theoretical g-mode frequencies between 10 and 250 μHz, which correspond to radial orders in the range $n = -46$ to -1 for modes with an angular degree $\ell = 1$ and 2. Indeed, our work focuses on the low-degree g-modes that have been searched for with the *SOHO* mission. These g-mode frequencies are obtained for different solar models, which we compare with the seismic one.

Section 2 describes these different solar models. Sound-speed and density profiles are compared to results derived from inversions of seismic observations. In § 3, we analyze how each physical process influences the predictions of g-mode frequencies, and we compare our results to other works of the helioseismology community. In § 4, we derive the sensitivity of different g-modes to the solar core rotation. In § 5, we discuss the recent detection of g-mode candidates in the light of this theoretical approach, and we comment on the g-mode excitation mechanisms. Finally, we summarize our results in § 6.

2. DESCRIPTIONS OF THE DIFFERENT SOLAR MODELS

Six models are computed using the CESAM code (Code d'Evolution Stellaire Adaptatif et Modulaire) developed by P. Morel (Morel 1997). This one-dimensional code solves the classical equations describing the stellar structure for a quasi-static stellar evolution. The solar models are computed for an age of 4.6 Gyr, including the pre-main sequence (starting 50 Myr before the Sun reached the zero-age main sequence). We use the recent OPAL equation of state, including relativistic effects for the electrons. The nuclear reaction rates result from the compilation of Adelberger et al. (1998) and include intermediate screening (Dzitko et al. 1995) when needed. The models are calibrated in luminosity, in radius, and in Z/X with a 10^{-5} relative accuracy (Z is the metal mass fraction, and X is the hydrogen mass fraction). The models using the Grevesse et al. (1993) composition are calibrated at $Z/X = 0.0245$ at the solar age, whereas the models with the new abundances of Asplund et al. (2005) are calibrated at $Z/X = 0.0172$. Here is the list of models produced for this paper:

1. A standard model without microscopic diffusion (hereafter the no-diffusion model).
2. A standard model including microscopic diffusion, without diffusion in the tachocline, and with the composition of Grevesse et al. (1993) (the std93 model).
3. A standard model with microscopic diffusion, without diffusion in the tachocline, and with the composition of Asplund et al. (2005) (the std05 model).
4. A standard model with microscopic diffusion, with diffusion in the tachocline (Brun et al. 1999), and with the composition of Grevesse et al. (1993) (the tacho93 model).
5. A standard model with microscopic diffusion, with diffusion in the tachocline, and with the composition of Asplund et al. (2005) (the tacho05 model).
6. The seismic model Seismic$_2$ from Couvidat et al. (2003a) (the seismic2 model), which includes relativistic effects for the electrons in the equation of state.

The prescription of Michaud & Proffitt (1993) is used for the treatment of microscopic diffusion. Some models include horizontal diffusion in the tachocline, as established by Spiegel & Zahn (1992). This diffusion process was first introduced in solar models by Brun et al. (1999), and then updated by Piau & Turck-Chièze (2002) with an improved description of the solar rotation profile in the pre-main sequence. The Brunt-Väissälä frequency is set at 25 μHz in the tachocline for the models tacho93 and tacho05, and the width of the tachocline is set at 0.05 $R_\odot$. In the two models based on the new solar abundances from Asplund et al. (2005), the opacities of the external layers (the atmosphere) had to be modified to account for this new chemical composition (following Turck-Chièze et al. 2004b). The new determination of the solar chemical composition is based on nonlocal thermodynamic equilibrium models of the solar atmosphere, three-dimensional simulations of stellar convection, and a better determination of the peaks in the solar spectrum. A major change accompanying this new composition is the reduction of the mass fraction of the CNO elements by about 30% in the Sun.

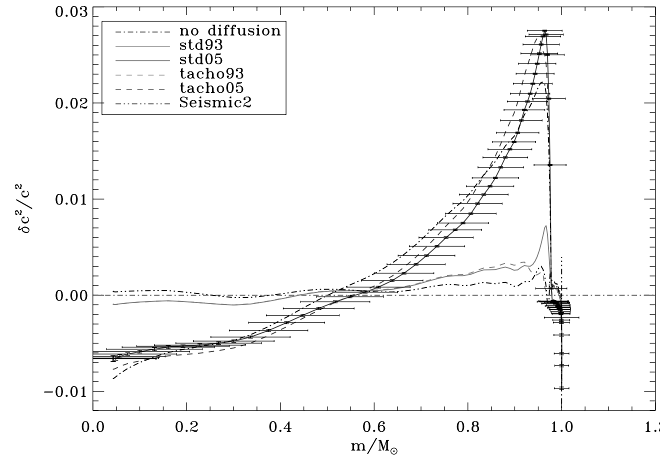

FIG. 1.—Difference in the squared sound-speed profiles between observations (Turck-Chièze et al. 2001; Couvidat et al. 2003a) and models, as a function of the solar mass. Gray curves and black solid and dashed curves correspond to the Grevesse et al. (1993) and Asplund et al. (2005) chemical compositions, respectively. The solid lines correspond to a model without horizontal diffusion in the tachocline, whereas the dashed lines correspond to a model with horizontal diffusion. The dot-dashed line is the model without microscopic diffusion, and the double-dot-dashed line is the seismic model. For clarity, the error bars have been plotted only on one model. [*See the electronic edition of the Journal for a color version of this figure.*]

All our solar models are one-dimensional, and therefore they do not take into account the dynamics of the solar interior. Also, we use the seismic model as a reference model, as it is halfway between the classical standard model and the dynamic model of the Sun. It is only a first step, however, before the development of a more sophisticated model that takes into account all the dynamic processes contributing to the solar internal rotation profile at 4.6 Gyr.

2.1. *Sound-Speed Profile*

For a study of the gravity-mode properties, the mass $m(r)$ seems to be the natural variable to use (instead of the radial distance to the solar center, r). In fact 98% of the total mass of the Sun is concentrated in the radiative interior. This choice of variable especially highlights the nuclear core, which makes up 60% of the mass of the Sun. Figure 1 shows the relative difference between the observed solar squared sound-speed profile (obtained from seismic data) and the theoretical one for our different solar models as a function of $m(r)$. This figure can be compared to the results already obtained by Turck-Chièze et al. (2004b), and Mathur et al. (2006). The large uncertainty in the radial location is due to the intrinsic properties of acoustic modes. We notice a difference as large as about 0.7% between the standard model std93 and the seismic observations in the vicinity of the tachocline. If we add horizontal diffusion in the tachocline, we manage to reduce this discrepancy (tacho93).

Solar models computed with the new chemical composition of Asplund et al. (2005) present a larger discrepancy between the observed sound speed and the sound speed derived from these models. This discrepancy is significant in the radiative zone and mainly reflects the role of the CNO elements in the opacity coefficients (in the range $r = 0.2\text{–}0.7\ R_\odot$). This discrepancy is even larger than the one obtained with our solar model without microscopic diffusion (the no-diffusion model), which is based on the abundances of Grevesse et al. (1993). Moreover, models with the abundances of Asplund et al. (2005) also exhibit a large discrepancy in the region below $0.15\ R_\odot$ as a consequence of the change in the CNO opacities and the slight variation in the Z/X ratio used for the calibration and in the CNO-cycle reaction rate in the solar core; both lead to a slight modification of the initial hydrogen mass fraction after calibration of the models. Finally, the seismic model exhibits, by definition, the best agreement with the observations.

2.2. *Density Profile*

If acoustic modes are adequate for determining the solar sound-speed profile, gravity modes are best used for determining the density profile in the radiative interior. Figure 2 (*top*) shows the relative difference in the solar density between observations and models as a function of $m(r)$. For the models using the abundances of Grevesse et al. (1993) this difference is lower than 2%, whereas for the models including the abundances of Asplund et al. (2005), this difference reaches 10% at $0.9\ M_\odot$. Moreover, the profiles for the std05 and tacho05 models seem to show a less dense core. A small density variation in the interior has a strong impact on the upper solar layers, because of the sharp drop in the density in the convection zone and because of the requirement that our models have solar mass. We notice that the resolution in mass is very poor for the observed solar density profile. It is likely to be improved only by the introduction of some g-mode frequencies in the inversion procedure.

Figure 2 (*bottom*) displays the difference between the density of the first five solar models listed in § 2 and the density of the seismic model for a radius r in the range $r = 0\text{–}0.2\ R_\odot$. This figure shows that the the no-diffusion model without microscopic diffusion presents the largest discrepancy. Conversely, the models with the Grevesse et al. (1993) abundances exhibit the smallest discrepancy, confirming what was seen with the sound-speed profiles.

3. INFLUENCE OF PHYSICAL INPUTS ON THE g-MODE FREQUENCIES

In this section, we show the sensitivity of the g-mode frequencies to physical processes in the models described previously and their asymptotic properties.

3.1. *Gravity-Mode Frequencies*

We derive the g-mode frequencies for the modes $\ell = 1$ and 2, from $n = -46$ to -1, for the seismic model. We use the adiabatic oscillation code of Aarhus University.[4] Obtaining accurate values for the g-mode frequencies over the large range 10–300 μHz requires that our solar model have enough layers sampling the nuclear core. Indeed, the high-order gravity modes are very sensitive to the structure of this core. Also, we choose a fine radial grid for seismic2 in order to properly sample the inner 5% in radius. Once this step is performed, we apply the oscillation code on a 2400 point grid, using the Richardson extrapolation to calculate the g-mode frequencies. These frequencies for the model seismic2 are listed in Table 1. This table illustrates the presence of a large number of modes at low frequency, which explains why it is difficult to label any potential g-mode candidate. Therefore, there is probably little hope to detect low-frequency g-modes individually, except with a very specific treatment. Moreover, even if these modes are detected, their amplitude might be too small for them to be useful. This is why it is better to look for the g-mode asymptotic behavior in this frequency range, as was done by García et al. (2007). We will discuss this point further in § 4.

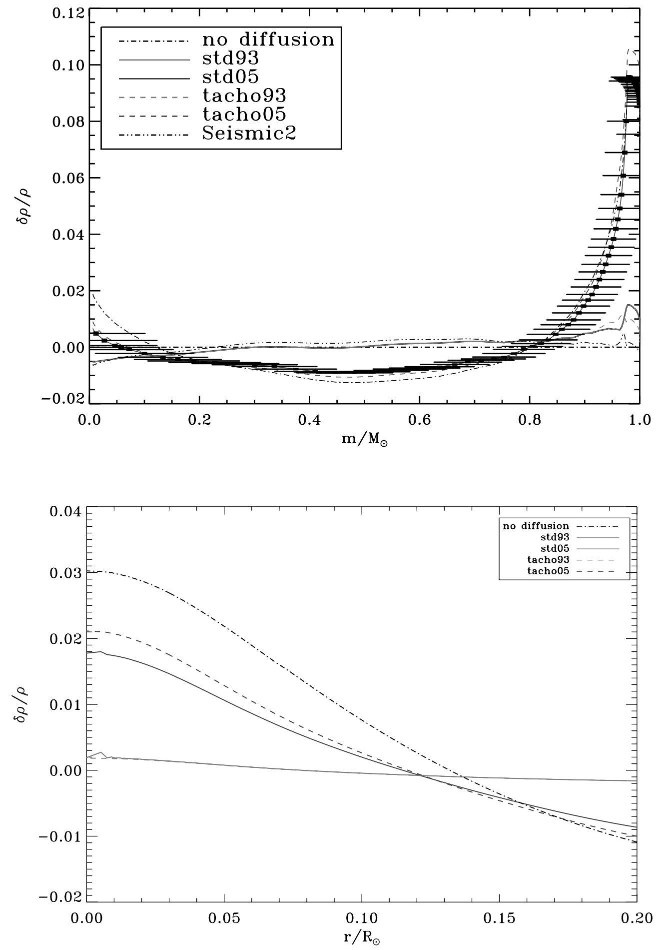

FIG. 2.— *Top*: Difference in the density profiles between observations (Couvidat et al. 2003a) and models, as a function of the mass. Same legend as Fig. 1 for the different lines. *Bottom*: Close-up of the nuclear region for the difference in the density profiles between the different models and the seismic model. [*See the electronic edition of the Journal for a color version of this figure.*]

The same g-mode frequency calculation was performed for the different solar models. The differences between the frequencies of the five models and the frequencies of the seismic model are shown in Figure 3 for $\ell = 1$ (*top*) and $\ell = 2$ (*bottom*). The main result is a conspicuous dependence of these differences on the mode frequency. In absolute value, these differences increase when the frequency increases. Therefore, the high-frequency g-modes are useful for discriminating between solar models. On the other hand, low-frequency modes (modes with a large radial order n in absolute value) are more sensitive to the physics of the inner core than high-frequency modes, as seen by their

[4] See the notes on the adiabatic oscillation programme by J. Christensen-Dalsgaard (http://www.phys.au.dk/~jcd/adipack.n/).

TABLE 1

List of g-Mode Frequencies for the Solar Model seismic2

$\ell = 1$				$\ell = 2$			
n	ν (μHz)	n	ν (μHz)	n	ν (μHz)	n	ν (μHz)
−46	14.6	−22	30.0	−46	24.9	−22	50.6
−45	14.9	−21	31.4	−45	25.5	−21	52.8
−44	15.3	−20	32.9	−44	26.0	−20	55.3
−43	15.6	−19	34.5	−43	26.6	−19	58.0
−42	16.0	−18	36.3	−42	27.2	−18	60.9
−41	16.4	−17	38.4	−41	27.9	−17	64.3
−40	16.8	−16	40.6	−40	28.5	−16	67.9
−39	17.2	−15	43.2	−39	29.2	−15	72.0
−38	17.7	−14	46.1	−38	29.9	−14	76.6
−37	18.1	−13	49.3	−37	30.8	−13	49.3
−36	18.6	−12	53.1	−36	31.6	−12	87.8
−35	19.1	−11	57.4	−35	32.5	−11	94.6
−34	19.7	−10	62.5	−34	33.4	−10	102.5
−33	20.2	−9	68.5	−33	34.3	−9	111.7
−32	20.9	−8	75.7	−32	35.4	−8	122.6
−31	21.5	−7	84.4	−31	36.5	−7	135.6
−30	22.2	−6	95.2	−30	37.6	−6	151.3
−29	22.9	−5	109.1	−29	38.9	−5	170.5
−28	23.8	−4	127.7	−28	40.2	−4	194.2
−27	24.6	−3	153.3	−27	41.6	−3	222.1
−26	25.5	−2	191.6	−26	43.2	−2	256.2
−25	26.5	−1	262.9	−25	44.8	−1	296.4
−24	27.6			−24	46.6		
−23	28.7			−23	48.5		

Note.—Values calculated for modes $\ell = 1$ and $\ell = 2$ and for $n = -46$ to -1.

eigenfunctions. Figure 3 mirrors the result of the comparison between models shown in Figures 1 and 2 in the nuclear core (see the bottom panel of Fig. 2 for the density profile). The change in slope of the curves in the two panels of Figure 3 highlights the difference between "pure" g-modes and mixed modes: mixed g-modes are also sensitive to the external solar layers, unlike pure g-modes. Almost all our solar models produce g-mode frequencies that agree at low frequency to within 0.5 μHz, while at high frequency the largest difference reaches 5 μHz.

To generalize this discussion, we compared our results with the results of other solar physics groups. Two comparisons were performed: first with a standard solar model, the widely used model S of Christensen-Dalsgaard et al. (1996), computed with a different stellar evolution code and an extraction of the g-mode frequencies based on the same pulsation code that we used; and second with the model M1 from Nice (Provost et al. 2000), which is rather similar to our standard model std93 because it is calculated with the same CESAM code. The g-mode frequencies for M1 were derived with a different pulsation code. Figure 4 of Mathur et al. (2006) illustrates the frequency differences for these models (compared to model seismic2) and for modes $\ell = 1$. This difference ranges from -0.1 to 0.45 μHz for model M1 and from -0.1 to 0.2 μHz for model S. Similar differences are observed for the modes $\ell = 2$. It is difficult to be specific regarding the origin of such differences; they are small and of the same order of magnitude as the differences we observe between our standard model and seismic2. We can nevertheless mention some small differences. The model from Nice is a calibrated model with a solar age of 4.65 Gyr and has no turbulent mixing below the convective zone. In the model S, relativistic effects were not yet introduced in the equation of state, and the nuclear processes are not treated in exactly the same way.

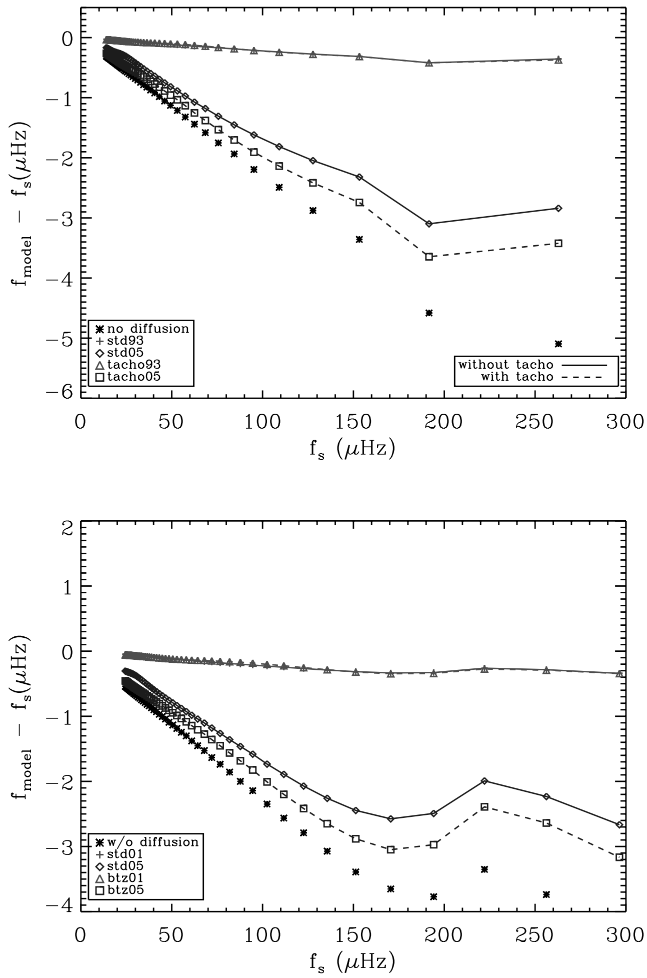

Fig. 3.—Difference between the g-mode frequencies from the five different solar models and the frequencies derived from the seismic model for $\ell = 1$ (*top*) and $\ell = 2$ (*bottom*). The solid line corresponds to a model without horizontal diffusion in the tachocline, whereas the dashed line corresponds to a model with horizontal diffusion. [*See the electronic edition of the Journal for a color version of this figure.*]

So far, the scope of this study has been limited to solar models based on the same physical hypotheses. Also, it seems useful to discuss the implementation of dynamic effects involving rotation, magnetic field, and gravity waves in the solar models. We mentioned in the introduction that these models are not yet available, even though some preliminary works already include some dynamic effects: transport of momentum by rotation and gravity waves (Talon & Charbonnel 2005; Charbonnel & Talon 2005) or the effect of the internal magnetic field on the internal rotation profile (Eggenberger et al. 2005), but these models are not sufficiently accurate to be compared in detail to the different helioseismic indicators. Therefore, gravity-mode frequencies have not been extracted from these models. Another approach followed by, e.g., Rashba et al. (2007) is to attempt to analytically estimate the direct effect of the rotation and of the magnetic field in the radiative region on the g-mode frequencies. For the specific cases studied in their paper, the authors found that the change in g-mode frequency is small and probably lower than 2 μHz for high-frequency modes. Preliminary studies show that the effects of momentum transport on the g-mode frequencies might be a little bit larger than the effects studied by Rashba et al. (2007), with the condition that these models must still reproduce the observed solar sound-speed profile. Therefore, the present study and the g-mode frequency differences are as realistic as possible and as

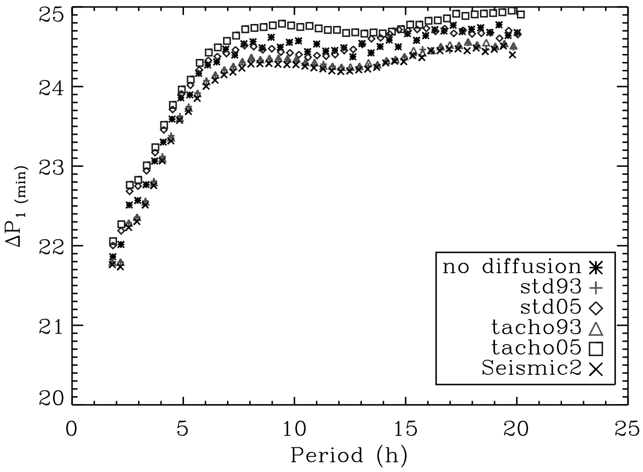

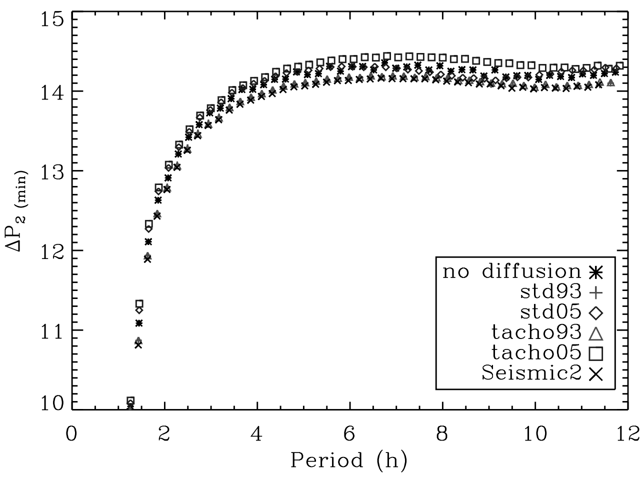

FIG. 4.—Comparison of the difference of P_ℓ between two g-modes of successive radial order (eq. [5]) derived with the oscillation code for the different solar models and for $\ell = 1$ (*top*) and $\ell = 2$ (*bottom*). Same legend as previous figures. The asymptotic value is between 24 and 25 minutes for the modes $\ell = 1$ and between 14 and 15 minutes for the modes $\ell = 2$. [*See the electronic edition of the Journal for a color version of this figure.*]

representative as possible of the uncertainties which are still present in the internal structure.

3.2. *The Asymptotic Properties*

In this section we study the asymptotic behavior of the g-modes for the different solar models listed in § 2. We base our calculations on Provost & Berthomieu (1986), who generalized the second-order asymptotic approximation to the solar case derived by Tassoul (1980). They showed that the g-mode frequencies are periodically spaced with the period ΔP_ℓ. In this approximation, we define the period $P_{n,l}$ of a mode of degree ℓ and radial order n as:

$$P_{n,\ell} = \frac{P_0}{2\sqrt{\ell(\ell+1)}}(2n+\ell+\phi) + \frac{P_0}{P_{n,\ell}} W_\ell, \qquad (1)$$

with

$$P_0 = 2\pi^2 \left(\int_0^{r_c} \frac{N}{r}\, dr \right)^{-1} \qquad (2)$$

and

$$W_\ell = V_1 + \frac{V_2}{\ell(\ell+1)}, \qquad (3)$$

TABLE 2

VALUES OF $P_{0(\mathrm{asym})}$ AND $\Delta P_{1(\mathrm{asym})}$ FOR DIFFERENT SOLAR MODELS

Solar Model	$P_{0(\mathrm{asym})}$ (minutes)	$\Delta P_{1(\mathrm{asym})}$ (minutes)
No diffusion	36.7	25.9
Std93	36.4	25.8
Tacho93	36.5	25.8
Std05	37.1	26.2
Tacho05	37	26.2
Seismic2	36.4	25.8

NOTE.—$\Delta P_{1(\mathrm{asym})}$ was obtained with eq. (4) and $P_{0(\mathrm{asym})}$ was derived with eq. (2).

where N is the Brunt-Väissälä frequency, r_c is the radius of the convective zone, ϕ is a phase factor that depends on n and ℓ, V_1 depends on N, and V_2 is a complex term. Using only the first order of equation (1), ΔP_1 (ΔP_ℓ for $\ell = 1$) is given by the relation

$$\Delta P_1 = P_{n+1,1} - P_{n,1} \simeq \frac{P_0}{\sqrt{2}}. \qquad (4)$$

The top and bottom panels of Figure 4 show these temporal differences ΔP_1 and ΔP_2, respectively, between two consecutive frequencies f for the solar models listed in § 2, where ΔP_1 was calculated as follows (instead of using eq. [4]):

$$\Delta P_1 = \frac{1}{f_{n+1,1}} - \frac{1}{f_{n,1}}. \qquad (5)$$

For all the models studied here, we notice that ΔP_1 reaches the asymptotic regime for g-mode periods greater than 5 hr (frequencies smaller than 55 μHz), and it varies between 24 and 25 minutes, while ΔP_2 varies between 14–15 minutes for g-modes with a period greater than 4 hr (frequencies smaller than 70 μHz).

Then we determined the theoretical values of P_0 (based on eq. [2]) and ΔP_1 (based on eq. [4]), which we called $P_{0(\mathrm{asym})}$ and $\Delta P_{1(\mathrm{asym})}$, respectively, and we compared these values with the ones derived from the frequencies returned by the adiabatic oscillation code (using eq. [5]). These different values are shown in Table 2 (for $P_{0(\mathrm{asym})}$ and $\Delta P_{1(\mathrm{asym})}$) and Table 3 (for $P_{0(\mathrm{osc})}$ and $\Delta P_{1(\mathrm{osc})}$). The difference between these two tables is of the order of 1–2 minutes and is due to the simplification of the expression in the calculation of Table 2. The major result of this study is that the values of ΔP_1, like those of P_0, are very similar for all our solar models: they agree to within a 1 minute range (even when models with the recent chemical composition are included). This

TABLE 3

VALUES OF $P_{0(\mathrm{osc})}$ AND $\Delta P_{1(\mathrm{osc})}$ FOR DIFFERENT SOLAR MODELS

Solar Model	$P_{0(\mathrm{osc})}$ (minutes)	$\Delta P_{1(\mathrm{osc})}$ (minutes)
No diffusion	34.7	24.6
Std93	34.5	24.4
Tacho93	34.5	24.4
Std05	34.7	24.6
Tacho05	35.1	24.8
Seismic2	34.4	24.3
Nice model	34.4	24.3
Model S	34.4	24.6

NOTE.—$\Delta P_{1(\mathrm{osc})}$ is the mean value of ΔP_1 calculated with the numerical frequencies returned by the adiabatic oscillation code, and $P_{0(\mathrm{osc})}$ is derived with eq. (4).

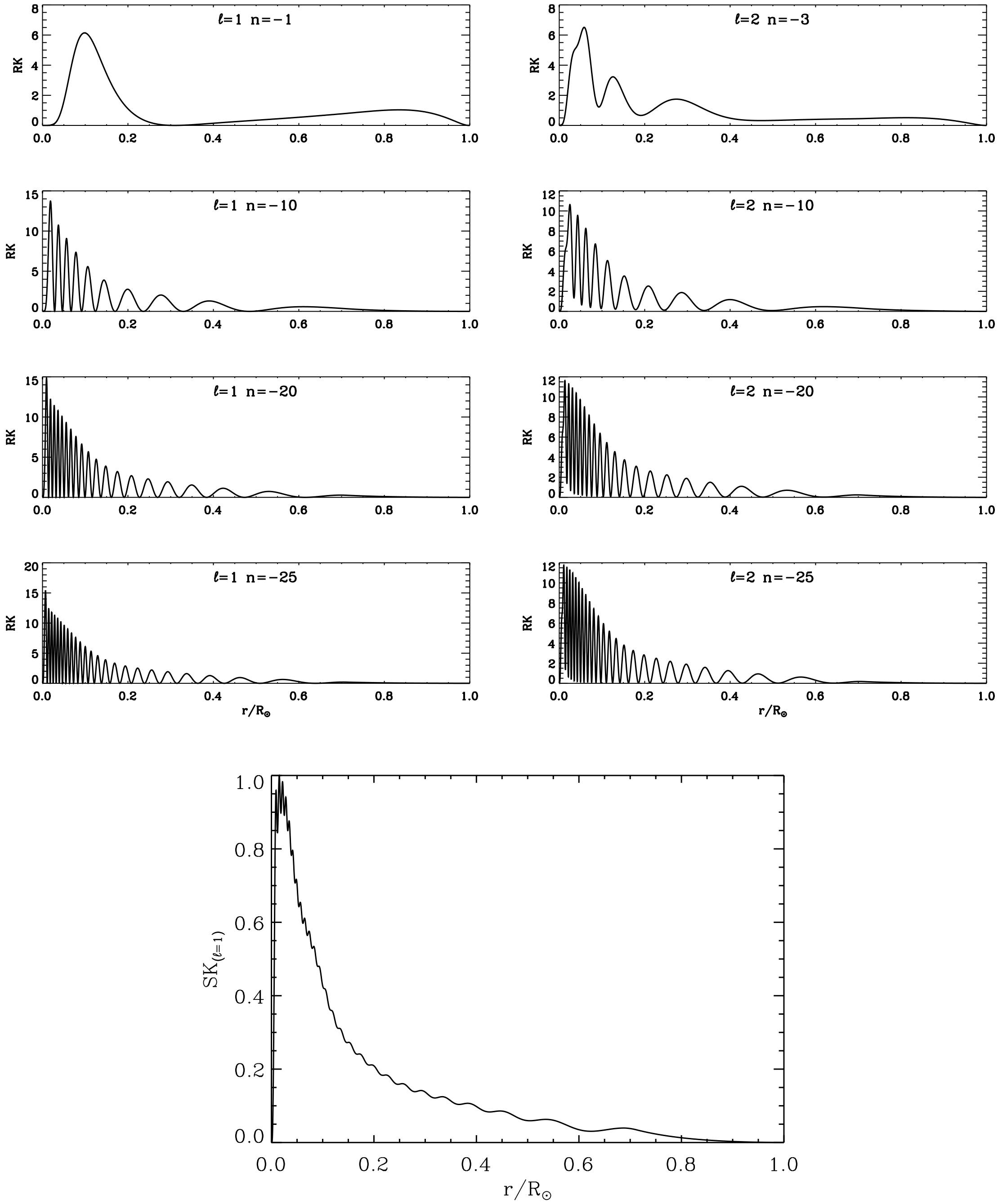

FIG. 5.—*Top*: Rotational kernels for a few $\ell = 1$ g-modes. These kernels were computed with the adiabatic oscillation code from Aarhus University. *Bottom*: Cumulative effect of the rotational kernels for $\ell = 1$, and for $n = -25$ to -4.

is a very significant improvement compared to the situation prior to the launch of the *SOHO* spacecraft, when variations of P_0 were in the range of 30 to 60 minutes (Hill et al. 1991). This improvement can mainly be traced to significant updates in the physics of the stellar models over the last 20 years. It also results from many comparisons between different solar evolution codes and from the incidence of helioseismic data on the quality of the solar models.

4. THE SENSITIVITY OF g-MODES TO THE ROTATION OF THE SOLAR CORE

The dynamics of a star manifests itself first through the stellar rotation profile. In the solar radiative zone, this profile is now known down to 0.3 $R_\odot$ thanks to the detection of low-order acoustic modes (Thompson et al. 2003; Couvidat et al. 2003b; García et al. 2004; Eff-Darwich et al. 2006). Gravity modes are needed if we want to infer the rotation profile closer to the solar center. Here we examine the sensitivity of different g-modes to the rotation of the nuclear core.

The perturbation in the mode frequency, $\Delta\nu_{n,\ell,m}$ (the rotational part of the frequency splitting between the mode components of azimuthal order $\pm m$ and of order n and degree ℓ), induced by the rotation of the Sun, $\Omega(r,\theta)$, is given by Thompson et al. (2003):

$$\Delta\nu_{n,\ell,m} = m \int_0^R \int_0^\pi K_{n,\ell,m}\Omega(r,\theta)\,dr\,d\theta, \qquad (6)$$

where $K_{n,\ell,m}(r,\theta)$ is the rotational kernel, and θ is the colatitude.

We first compute some kernels $K_{n,\ell,m}(r,\theta)$ for the model seismic2. Figure 5 (*top*) shows the sensitivity of these kernels to the rotation of the nuclear core (except in the case $\ell = 1$, $n = -1$), and how it increases with n. Moreover, when we consider the cumulative effect of the dipolar modes with a radial order ranging from $n = -25$ to -4 (bottom panel of Fig. 5), as was done by García et al. (2007), we find that the influence of the inner core is increased. Indeed, we estimate that 65% of the rotational splitting of these modes come from the region below 0.2 $R_\odot$. This has to be compared with, e.g., the mode $\ell = 2$, $n = -3$, for which we also notice a great influence of the core rotation rate on the splitting, but this influence is more localized above 0.05 $R_\odot$, with 53% of the rotational splitting coming from the region between 0 and 0.2 $R_\odot$ and only 34% coming from the very inner core (below 0.1 $R_\odot$). One can infer the solar rotation profile as a function of radius and latitude from a set of observed rotational frequency splittings. This work is in progress and will be published soon.

5. ON THE g-MODE OBSERVATIONS

A breakthrough in the physics of the radiative interior should come from the detection of gravity modes. In the previous sections we identify several characteristics of g-modes which are useful in interpreting the recent potential g-mode observations. To date, two methods resulted in the detection of g-mode candidates with the GOLF instrument.

The first method, described in Turck-Chièze et al. (2004a, 2004c), consists of searching for multiplets (several components equally spaced in frequency and belonging to the same mode) in the high-frequency domain of the gravity-mode power spectrum, where individual modes can be identified. By looking for multiplets instead of a single spike, the threshold of detection for a given statistical significance is decreased at a level compatible with the theoretical amplitude of the modes (Gough 1985; Andersen 1996; Kumar et al. 1996; Appourchaux 2003). Any dubious detection can be rejected by comparing the frequency of the detected pattern with the theoretical frequencies derived from solar models. In this method, it is often difficult to label the observed pattern without ambiguity.

The second method, described in García et al. (2006, 2007), is adapted to the low-frequency range of the g-mode spectrum. Indeed, the expected mode amplitude is so small in this frequency range that any individual detection has been ruled out. Although this kind of individual search was favored in the past (Hill et al. 1991), it now seems that only an investigation of the general properties of the g-modes through their asymptotic behavior might produce some results and allow a proper labeling of the observed signature.

5.1. *The High-Frequency g-Mode Range*

The detection of high-frequency g-modes should improve the solar density profile and better constrain some physical phenomena that have not yet been included in the solar models. In the frequency range 150–450 μHz, several multiplet candidates have been identified, and their evolution over time has been followed. Figure 6 recalls the temporal evolution of the most interesting case, published in 2004. In a 10 μHz range, after 1290 days of observation, a triplet (three peaks) was detected with a confidence level of 98%. If we also consider the fourth peak visible to the left of the triplet as a part of the same mode, we can conclude that a quadruplet was detected. After 2975 days of observation, a peak emerged halfway between the two left peaks of this quadruplet (see bottom panel of Fig. 6); therefore this structure was considered a quintuplet with a confidence level higher than 98%. The simplest choice to label such a pattern (if it is a gravity mode) is to identify it with a mode $\ell = 2$, $n = -3$. Indeed, this g-mode candidate has a central frequency in agreement with the theoretical frequency derived from seismic2 for $\ell = 2$, $n = -3$ within 2 μHz. This difference cannot be explained only by the presence of a magnetic field in the central region of the Sun, since the sign of this difference is opposite to what is expected, and the effect smaller (see Rashba et al. 2007), but the present study shows differences up to 5 μHz depending on the considered models. Only a complete solar dynamic model will finally decide this case. Indeed, the detection of a quintuplet for $\ell = 2$, $n = -3$ instead of the expected triplet could mean a different rotation axis for the central core of the Sun in comparison to the rest of the Sun, as well as a rapidly rotating core, due to the rotational splitting of 0.6 μHz that this quintuplet implies. The identification of the pattern as a mode $\ell = 2$, $n = -3$ is supported by the work of Cox & Guzik (2004) on the excitation of gravity modes. However, this identification remains uncertain due to the theoretical prediction of modes $\ell = 3$ and 5 in the vicinity of the $\ell = 2$; therefore, the detection of a mixture of modes cannot be excluded. If the pattern is a triplet mixed with other modes, this would favor a flat rotation

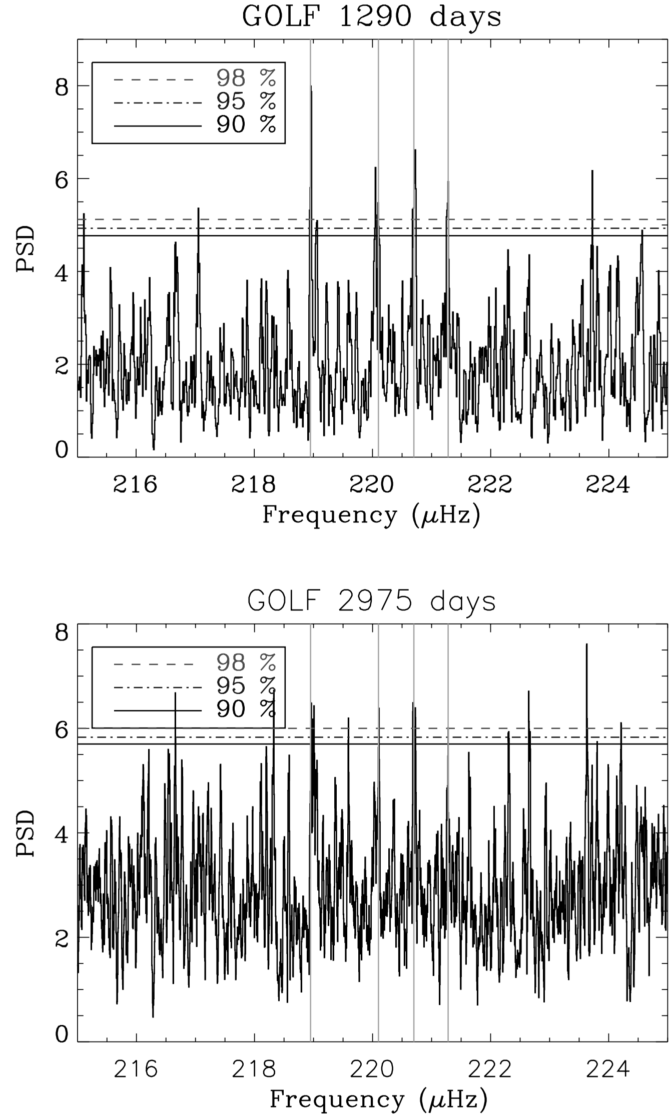

FIG. 6.—Quadruplet detected above the 98% confidence level inside a 10 μHz box (the confidence level is the probability for the structure not to be produced by pure noise) after 1290 days (*top*), and a quintuplet detected after 2975 days (*bottom*) with the same confidence level in the multitaper analysis. The peaks detected in the previous analysis of Turck-Chièze et al. (2004a) are superimposed on the two figures. [*See the electronic edition of the Journal for a color version of this figure.*]

profile in the solar core, in apparent contradiction to the detections at low frequency (see below).

5.2. *The Low-Frequency Range*

In § 3 we emphasized that the gravity modes have a specific asymptotic behavior in the low-frequency range. We showed that below 100 μHz, the absolute frequency of the g-modes is not significantly influenced by the physics of the solar core included in our solar models. This is likely to be an asset, because it makes it possible to label any signal detected with the expected frequency without ambiguity. The second method to search for g-modes uses their asymptotic property: looking for differences between modes of consecutive radial orders n and using the cumulative effect of a large number of radial orders. With this method, Garcia et al. (2007) detected a signature of dipolar gravity modes. Although this frequency range is not currently very useful for improving the solar density profile, we pointed out in § 4 that these modes are very interesting in that they can constrain the rotation rate of the very inner core, which has been estimated to be greater than that of the rest of the Sun.

A preliminary study of the rotational splittings of several modes with different rotation profiles that are expected to have a realistic trend, i.e., with a core rotating faster than the rest of the radiative region, shows that the two g-mode detection methods at low and high frequencies produced results that agree with each other if the rotation of the core below 0.15 $R_\odot$ is 3 to 5 times larger than the rest of the radiative zone.

5.3. *The Excitation of the Observed Gravity Modes*

To date, the excitation characteristics of the gravity modes have not been clearly established. It was generally thought that these modes are excited by the granulation pattern of the convective zone, in a fashion similar to the acoustic modes (Goldreich & Kumar 1990). As a consequence, their lifetime was supposed to be very long (several years and even millions of years) and their amplitude very small (making them theoretically undetectable with the instruments on board *SOHO*). More recently, another hypothesis was suggested by Garciá-López & Spruit (1991) and Dintrans et al. (2005): these modes could be excited by some penetrative convective plumes at the base of the convective zone. As a consequence, their lifetime would be reduced, and their amplitude might be different from what was expected. Neither of our two g-mode detection methods favors pure stable modes, which are expected to have a very thin line width and an amplitude increasing with time, as observed for the low-order acoustic modes such as the case $\ell = 0$ and $n = 6$. So far, the results of these two methods are compatible with g-modes whose power is distributed among several components. The asymptotic analysis would suggest a rather high signal-to-noise ratio, which is not observed, and the detected signature can be explained only if the power of the modes is dispersed in different spikes. Such behavior may be due to the re-excitation of the modes. For the candidate around 220 μHz, several spikes are clearly visible in the Fourier transform spectrum (and also in the multitaper analysis shown in Fig. 6). We examined whether such a hyperfine structure could be provoked by surface solar cycle effects (the analysis is done over 8 years). We computed the g-mode frequencies for solar models whose radius varies (according to what the *f*-mode data suggest). A relative change in the solar radius by about 10^{-4} during the solar cycle influences the gravity modes in the high-frequency range by no more than 10 nHz. Therefore, this effect appears too small to explain the observed hyperfine structure. So, if one can confirm that this candidate is a gravity mode, such behavior could provide important information about the existence of a magnetic field in the solar core (Goode & Thompson 1992; Rashba et al. 2007; Turck-Chièze et al. 2005b), or about the fact that the cavity where the mode is trapped slightly changes with time.

6. CONCLUDING REMARKS

This paper shows the respective interest of the different frequency ranges where gravity modes could be detected. We computed solar models with different combinations of physical processes. For each model we calculated g-mode frequencies for modes with $\ell = 1$ and 2 and $n = -46$ to -1. The comparison of these frequencies with a reference solar model (seismic2) showed the importance of the high-frequency modes, which have a sizable sensitivity to the physics of the solar core. Moreover, an analysis of the asymptotic behavior of g-modes at low frequency made it possible to conclude that the different solar models constrain the asymptotic value of ΔP_ℓ to within a 1 minute range.

The analysis of the rotational kernels of seismic2 also showed at which level the g-modes are sensitive to the rotation rate of the solar regions below 0.2 $R_\odot$, and how the two-frequency range analysis could be coherent.

The g-modes in the high-frequency range are mainly influenced by the density and the sound speed in the solar core. This core makes up almost 60% of the solar mass. If we ever manage to determine the precise central frequency of one or two g-modes, this information will help us constrain the additional physical phenomena that we would like to introduce in a dynamic solar model. A measure of the frequency splitting of these individual modes should be useful to probe the solar core. The high density of modes of different angular degrees in a small range of frequencies (typically within 10 μHz) favors the development of masks in front of the next generation of helioseismic instruments, in order to avoid dubious identifications (Turck-Chièze et al. 2006). This study emphasizes the importance of the identification of the pattern observed in this range of frequencies (if attributed to g-modes).

In the low-frequency range of the power spectrum, the physics of the solar models seems rather well constrained, making it possible to identify the angular degree ℓ of the modes that might be detected without ambiguity (by looking at the separation between adjacent radial orders n). Consequently, the signature of the dipolar gravity modes with the GOLF instrument seems well established. Moreover, we can potentially constrain the innermost rotation rate. Such an analysis at low frequency will be pursued not only for $\ell = 1$, but also for $\ell = 2$, to derive a realistic rotation profile inside the solar core.

An important issue is the understanding of how such modes are excited: the power of the g-mode candidates we detected seems distributed over several bins, a fact difficult to explain by the presence of a central magnetic field or by fluctuations of the solar outer layers. This power distribution favors the idea that the modes are excited at the base of the convective zone, and that this turbulent layer could spread the signal into several spikes or re-excite the g-modes.

Here we show several interesting characteristics of gravity modes. Combined with the unambiguous detection of some of these gravity-mode properties, this paper favors further works to finally derive the dynamics of the nuclear core.

We would like to thank Janine Provost and Jorgen Christensen-Dalsgaard for giving us access to their gravity-mode predictions in the range of frequencies we studied. Sébastien Couvidat was supported for his contribution by NASA grant NNG05GH14G (SOI/MDI).

REFERENCES

Adelberger, E., et al. 1998, Rev. Mod. Phys., 70, 1265
Andersen, B. 1996, A&A, 312, 610
Appourchaux, T. 2003, in Proc. SOHO 12/GONG+ 2002, Local and Global Helioseismology: The Present and Future, ed. H. Sawaya-Lacoste (ESA SP-517; Noordwijk: ESA), 131
Appourchaux, T., et al. 2000, ApJ, 538, 401
Asplund, M., Grevesse, N., & Sauval, A. J. 2005, in ASP Conf. Ser. 336, Cosmic Abundances as Records of Stellar Evolution and Nucleosynthesis in honor of David L. Lambert, ed. T. G. Barnes III & F. N. Bash (San Francisco: ASP), 25
Brun, A. S., Turck-Chièze, S., & Morel, P. 1998, ApJ, 506, 913
Brun, A. S., Turck-Chièze, S., & Zahn, J. P. 1999, ApJ, 525, 1032
Brun, A. S., & Zahn, J. P. 2006, A&A, 457, 665
Charbonnel, C., & Talon, S. 2005, Science, 309, 2189
Christensen-Dalsgaard, J., Proffitt, C. R., Thompson, M. J. 1993, ApJ, 403, L75
Christensen-Dalsgaard, J., et al. 1996, Science, 272, 1286
Couvidat, S., Turck-Chièze, S., & Kosovichev, A. G. 2003a, ApJ, 599, 1434
Couvidat, S., et al. 2003b, ApJ, 597, L77
Cox, A., & Guzik, J. 2004, ApJ, 613, L169
Dintrans, B., Brandenburg, A., Nordlund, Å., & Stein, R. F. 2005, A&A, 438, 365
Dzitko, H., & Turck-Chièze, S. 1995, ApJ, 447, 428
Eff-Darwich, A., Korzennik, S. G., Jiménez-Reyes, S., García, R. A. 2006, in Proc. SOHO 18/GONG 2006/HELAS I, Beyond the Spherical Sun, ed. K. Fletcher (ESA SP-624; Noordwijk: ESA), 84
Eggenberger, P., Maeder, A., & Meynet, G. 2005, A&A, 440, L9
Gabriel, A. H., et al. 2002, A&A, 390, 1119
García, R. A., Jiménez-Reyes, S., Turck-Chièze, S., Ballot, J., & Henney, C. J. 2004, in Proc. SOHO 14/GONG 2004, Helio- and Asteroseismology: Towards a Golden Future, ed. D. Danesy (ESA SP-559; Noordwijk: ESA), 436
García, R. A., Turck-Chièze, S., Jiménez-Reyes, S., Ballot, J., Pallé, P. L., Eff-Darwich, A., Mathur, S., & Provost, J. 2006, in Proc. SOHO 18/GONG 2006/HELAS I, Beyond the Spherical Sun, ed. K. Fletcher (ESA SP-624; Noordwijk: ESA), 23
———. 2007, Science, 316, 1591
García-Lopez, R. & Spruit H. 1991, ApJ, 377, 268
Goldreich, P., & Kumar, P. 1990, ApJ, 363, 694
Goode, P. R., & Thompson, M. J. 1992, ApJ, 395, 307
Gough, D. 1985, in Future Missions in Solar, Heliospheric and Space Plasma Physics, ed. E. Rolfe & B. Battrick (ESA SP-235; Noordwijk: ESA), 183
Grevesse, N., Noels, A., & Sauval, A. J. 1993, A&A, 271, 587
Hill, F., Froehlich, C., Gabriel, M., & Kotov, V. A. 1991, in Solar Interior and Atmosphere, ed. A. N. Cox, W. C. Livingston, & M. S. Matthews (Tucson: Univ. Arizona Press), 562
Iglesias, C. A., & Rogers, F. J. 1996, ApJ, 464, 943
Kumar, P., Quataert, E. J., & Bahcall, J. N. 1996, ApJ, 458, L83
Mathis, S., & Zahn, J.-P. 2004, A&A, 425, 229
———. 2005, A&A, 440, 653
Mathur, S., Turck-Chièze, S., Couvidat, S., García, R. A. 2006, in Proc. SOHO 18/GONG 2006/HELAS I, Beyond the Spherical Sun, ed. K. Fletcher (ESA SP-624; Noordwijk: ESA), 95
Michaud, G., & Proffitt, C. R. 1993, in IAU Colloq. 137, Inside the Stars, ed. W. W.Weiss & A. Baglin (San Francisco: ASP), 246
Morel, P. 1997, A&AS, 124, 597
Palacios, A., Talon, S., Turck-Chièze, S., & Charbonnel, C. 2006 in Proc. SOHO 18/GONG 2006/HELAS I, Beyond the Spherical Sun, ed. K. Fletcher (ESA SP-624; Noordwijk: ESA), 38
Piau L. & Turck-Chièze S. 2002, ApJ, 566, 419
Provost, J., & Berthomieu, G. 1986, A&A, 165, 218
Provost, J., Berthomieu, G., & Morel, P. 2000, A&A, 353, 775
Rashba, T. I., Semikoz, V. B., Turck-Chièze, S., & Valle, J. W. F. 2007, MNRAS, 377, 453
Rogers, F. J., & Iglesias, C. A. 1994, Science, 263, 50
Shibahashi, H., & Tamura, S., in Proc. SOHO 18/GONG 2006/HELAS I, Beyond the Spherical Sun, ed. K. Fletcher (ESA SP-624; Noordwijk: ESA), 81
Spiegel E. A., Zahn, J. P. 1992, A&A, 265, 106
Talon, S., & Charbonnel, C. 2005, A&A, 440, 981
Tassoul, M. 1980, ApJS, 43, 469
Thompson, M. J., Christensen-Dalsgaard, J., Miesch, M. S., Toomre, J., 2003, ARA&A, 41, 599
Thoul, A., Bahcall, J. N. and Loeb, A. 1994, ApJ, 421, 828
Turck-Chièze, S. 2005a, NuPhS, 143, 35
———. 2005b, NuPhS, 145, 17
———. 2006, Adv. Space Res, 37, 1569
Turck-Chièze, S., Couvidat, S., & Piau, L. 2005a, in Element Stratification in Stars: 40 Years of Atomic Diffusion, ed. G. Alecian, O. Richard, & S. Vauclair (EAS Publ. Ser. 17; Les Ulis: EDP Sci.), 149
Turck-Chièze, S., & Talon, S. 2007, Adv. Space Res., in press
Turck-Chièze, S., et al. 2001, ApJ, 555, L69
———. 2004a, ApJ, 604, 455 (erratum 608, 610)
———. 2004b, Phys. Rev. Lett, 93, 1102
———. 2004c, in Proc. SOHO 14/GONG 2004, Helio- and Asteroseismology: Towards a Golden Future, ed. D. Danesy (ESA SP-559; Noordwijk: ESA), 85
———. 2005b, in Trends in Space Science and Cosmic Vision 2020, ed. F. Favata et al. (ESA-SP 588; Noordwijk: ESA), 193
———. 2006, in Proc. SOHO 18/GONG 2006/HELAS I, Beyond the Spherical Sun, ed. K. Fletcher (ESA SP-624; Noordwijk: ESA), 24